Vol. 559: 45–63, 2016
doi: 10.3354/meps11883

MARINE ECOLOGY PROGRESS SERIES
Mar Ecol Prog Ser

Published November 9[§]

Coral growth, bioerosion, and secondary accretion of living orbicellid corals from mesophotic reefs in the US Virgin Islands

D. K. Weinstein[1,2,6,*], A. Sharifi[1,3], J. S. Klaus[1,2], T. B. Smith[4], S. J. Giri[1], K. P. Helmle[5]

[1]Department of Marine Geosciences, Rosenstiel School of Marine and Atmospheric Science, University of Miami, 4600 Rickenbacker Causeway, Miami, FL 33149, USA

[2]Department of Geological Sciences, University of Miami, Cox Science Building, 1301 Memorial Drive, Coral Gables, FL 33124, USA

[3]Neptune Isotope Laboratory (NIL), Department of Marine Geosciences, Rosenstiel School of Marine and Atmospheric Science, University of Miami, 4600 Rickenbacker Causeway, Miami, FL 33149, USA

[4]Center for Marine and Environmental Studies, University of the Virgin Islands, 2 John Brewer's Bay, St. Thomas, Virgin Islands 00802, USA

[5]Oceanographic Center, Nova Southeastern University, 8000 North Ocean Drive, Dania Beach, FL 33004, USA

[6]*Present address:* Department of Chemistry, Biology and Marine Science, University of the Ryukyus, 1 Senbaru, Nishihara, Okinawa 903-0213, Japan

ABSTRACT: Growth rates of the major Caribbean reef framework-building coral *Orbicella* spp. decrease with increasing water depth and light attenuation. However, reliable, spatially distributed growth rates for corals deeper than 30 m are rare, and the combined influence of coral framework accretion, secondary framework accretion, and framework macroboring on net framework calcification in these habitats is poorly constrained. To better understand the growth limits and spatial variability of *Orbicella*-dominated mesophotic coral reef ecosystems, live platy samples of *Orbicella franksi* were collected at 3 upper mesophotic reef habitats with varying structural characteristics on the Puerto Rican Shelf, south of St. Thomas, US Virgin Islands. Average mesophotic coral linear extension rates, determined by standard X-radiographic techniques and confirmed by stable isotopic analyses, were 0.80 ± 0.03 mm yr^{-1} (±SE), slower than previously recorded for *Orbicella* spp. at shallower US Virgin Island reefs. However, coral cover at 2 of the mesophotic reefs was considerably higher than at nearby shallow-water St. Thomas reefs, implying that fast coral growth rates are not necessarily needed to maintain Caribbean reefs with high coral cover and structural complexity. A probable reason for this is reduced bioerosion with depth. Rates of net coral framework calcification were significantly different between the neighboring mesophotic coral reef habitats, likely a result of the complex interplay between site variability in irradiance, nutrient availability, and other factors. Analysis also indicated that the influence of El Niño–Southern Oscillation on water circulation and salinity as well as on water clarity and nutrient distribution in the Caribbean is reflected in the annual variability of mesophotic *O. franksi* growth rates. Site differences in net coral framework calcification suggest a potential long-term mechanism for the production or maintenance of heterogeneous reef-scale geomorphology along broad-sloping carbonate shelves colonized with mesophotic coral reef systems.

KEY WORDS: Mesophotic coral ecosystem · Coral growth rate · Bioerosion · Secondary accretion · US Virgin Islands · *Orbicella* · Calcification · Skeletal carbon and oxygen stable isotope analysis · X-radiography · Density bands

INTRODUCTION

The physical foundation of a coral reef is dependent on the calcification of framework-building organisms (Stearn & Scoffin 1977, Scoffin et al. 1980, Perry et al. 2008). The combined variation of coral growth rates and *in situ* coral bioerosion rates influence reef complexity and structural sustainability, biodiversity, and

*Corresponding author: dweinstein@rsmas.miami.edu

[§]Corrections were made after publication. For details see www.int-res.com/articles/meps_oa/m619p215.pdf
This updated version: June 4, 2019

geomorphology (Roberts & Ormond 1987, Perry et al. 2008, Dustan et al. 2013). Differences in growth rates and calcification are caused by deviation in numerous factors such as temperature, light intensity (and depth), aragonite saturation state, nutrients and particulate matter, turbidity (see review by Pratchett et al. 2015), and *Symbiodinium* genotypes (Little et al. 2004, Jones & Berkelmans 2010, Pettay et al. 2015).

Orbicella spp. has been recognized as one of the most important reef-building corals in the Atlantic (Goreau 1959, Bosscher & Meesters 1993). Studies employing various techniques found that linear extension rates of *Orbicella* spp. decrease with increasing depth (Dustan 1975, Hubbard & Scaturo 1985, Bosscher & Meesters 1993), often attributed to decreasing levels of photosynthetically active radiation (PAR) (Bosscher & Meesters 1993). The results of these and other studies include data obtained from a limited number of mesophotic coral reef sites that sampled *Orbicella* spp. at deeper, steep-shelf habitats such as 36.6 m in St. Croix, US Virgin Islands (USVI) (Hubbard & Scaturo 1985), 44.1 m in Barbados (Runnalls & Coleman 2003), and 45 m in Jamaica (Dustan 1975). Other studies also found that *Orbicella* spp. skeletal density increases with increasing depth (Baker & Weber 1975, Hughes 1987).

Mesophotic coral ecosystems (MCEs), defined as deep (30 to 150 m) hermatypic zooxanthellate coral-dominated communities, are valued as highly biodiverse habitats with possible connectivity to shallow-water reefs (Riegl & Piller 2003, Bongaerts et al. 2010, Slattery et al. 2011, Holstein et al. 2015). MCEs typically form along slopes or platforms, often on pre-existing terraces and ridges (Locker et al. 2010). Steep, high-angle mesophotic reef structures form on the shelf break of continental and insular slopes (e.g. off Jamaica and Belize; Goreau & Land 1974, James & Ginsburg 1979). Mesophotic reef structures along platforms form on low-angle outer continental and insular shelves (e.g. off the Australian Great Barrier Reef and Okinawa, Japan; Harris et al. 2013, White et al. 2013). Mesophotic reefs can also be found on both platforms and slopes of submerged banks. Bathymetric studies suggest mesophotic reefs could exceed the spatial extent of shallow-water coral reefs (Locker et al. 2010, Bridge et al. 2012), with the Great Barrier Reef Marine Park coral reef habitat potentially underestimated by up to 100% (Harris et al. 2013).

Past studies to obtain Caribbean mesophotic coral growth rates (Dustan 1975, Hubbard & Scaturo 1985, Huston 1985, Runnalls & Coleman 2003) were limited in spatial coverage to one or a few deep sites, and to only slope geomorphological habitats. Therefore, there are limited studies to determine the degree of homogeneous lateral deposition along a large proportion of insular carbonate shelves. Additionally, little data are available regarding the growth and erosion of coral on low-angle mesophotic coral reefs.

Here we quantified the variability of coral growth rates and of framework secondary accretion and bioerosion rates from upper mesophotic coral reef (30 to 60 m; Slattery et al. 2011) Caribbean habitats. Specifically, we tested the following for the present-day mesophotic coral *Orbicella franksi*: (1) whether linear growth rates in the USVI were similar to growth rates published in the past for the same coral genus at similar depths in the Caribbean and at shallower reef sites; and (2) whether total net framework growth rates (calcification and secondary accretion less bioerosion) were the same at neighboring reefs with varying geomorphological characteristics at similar depths. Linear growth rates and bulk density were obtained with standard X-radiography and buoyancy weight techniques, respectively, and bioerosion and accretion rates were quantified through point count analysis. Skeletal isotopic compositions of corals were used to understand the physiological ecology of the mesophotic corals (Lesser et al. 2010), and demonstrate the correlation between *O. franksi* annual variability in growth rates and changes in skeletal $\delta^{13}C$ and $\delta^{18}O$. Periodic changes in coral growth rates (as reflected by luminance) were also compared with the Southern Oscillation Index (SOI) to investigate the potential controlling role of the El Niño–Southern Oscillation (ENSO) on environmental conditions in USVI mesophotic coral. Overall results from this study indicated that the combination of carbonate producing and eroding processes on mesophotic coral framework are significantly different between sites. When amplified over long timescales, these results could suggest that mesophotic coral reef carbonate deposition is more heterogeneous than previously assumed on low-angle shelves.

MATERIALS AND METHODS

Study sites

The upper mesophotic coral reefs between the northern USVI and the Anegada Passage create a large carbonate depositional environment atop the low-angle Puerto Rican Shelf, with up to 50% coral cover in some locations (Smith et al. 2010). A total of 3 sites with differing geomorphologies (Smith et al. 2010, Weinstein et al. 2014) were selected for analysis

(Fig. 1): (1) the Secondary Bank site (30.7 m); (2) the Primary Bank site (39.0 m); and (3) the Deep Flat Basin site (43.3 m). The Bank sites are atop long, elevated ridges with relief greater than 5 m and are aligned parallel to the Anegada Passage for more than 1 km. The Primary Bank is closest to the shelf edge and narrower than the more gently sloping, broader Secondary Bank (Fig. 1b). More detailed descriptions of these 2 sites are provided by Weinstein et al. (2015). The northern edge of the Secondary Bank transitions to a basin encompassing both the Hillock Basin (Smith et al. 2010, Weinstein et al. 2014) and the Deep Flat Basin habitats. The Deep Flat Basin is best characterized as an unbroken, flat expanse of coral pillars that rise to a consistent height of 0.5 to 1.0 m above the seafloor (Fig. 1f).

In August 2011, technical divers collected platy (flattened morphology; Dustan 1975) *Orbicella franksi* samples at the 3 sites. A hammer and chisel were used at each site to remove 10 samples, approximately 5 to 10 cm in diameter, from the outer edges (representing the youngest portion of the coral) of different, random, opportunistically selected colonies. The corals collected were identified as *O.*

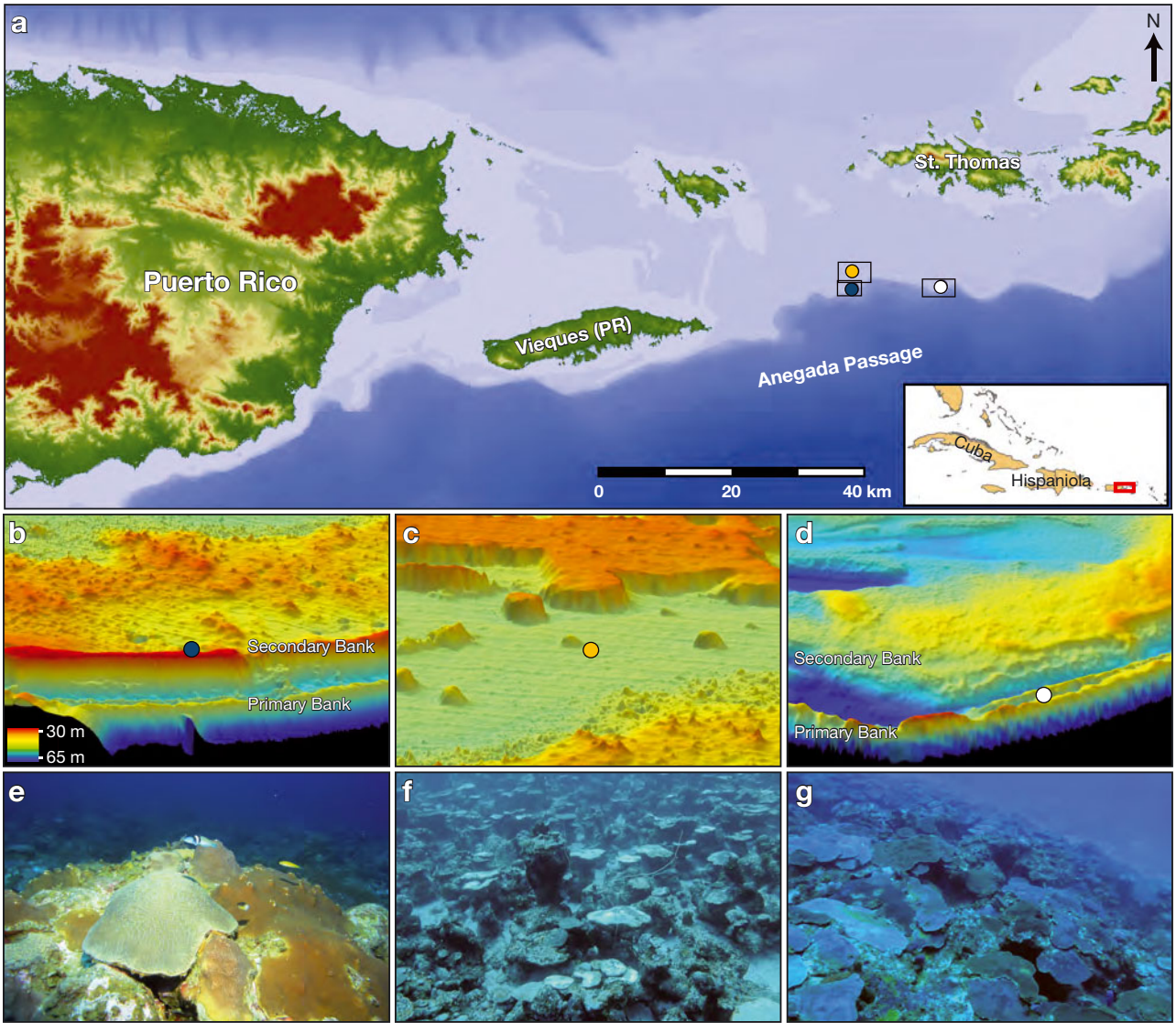

Fig. 1. South Puerto Rican Shelf study area, indicated by inset map (red box). (a) Locations of the Deep Flat Basin site (orange circle), Secondary Bank site (blue circle), and Primary Bank site (white circle). Black rectangles in (a) indicate location of bathymetry maps, with ×10 vertical exaggeration of the (b) Secondary Bank, (c) Deep Flat Basin, and (c) Primary Bank sites. Bathymetry data from Rivera et al. (2006) and NOAA Center for Coastal Monitoring and Assessment (https://coastalscience.noaa.gov/research/scem/seafloormapping). Color bar in (b) applies to all bathymetry maps. (e–g) Representative reefscape pictures of the (e) Secondary Bank, (f) Deep Flat Basin, and (g) Primary Bank

franksi based on their macroscopic structure. Platy *O. franksi* was selected because it is the most dominant coral type in bank mesophotic coral reefs of the northern USVI (>90% relative coral cover; Smith et al. 2010). Deeper sites were not sampled because *O. franksi* is rarely encountered below 45 m (Smith et al. 2014). Collected samples were soaked in a 50% solution of a commercial bleach product for 1 d, rinsed in distilled water for 1 d, and dried in an oven at 55°C for 2 d. Samples large enough for precision sectioning with a circular saw were cut into slices ~2 to 5 mm thick, parallel to the primary coral growth axis. Preliminary analysis indicated that Caribbean mesophotic corals are denser than the same species from shallower locations (Barnes & Devereux 1988, Helmle et al. 2011), so thin slices (only 1 corallite wide) were needed to ensure X-ray penetration and maximum clarity of banding.

Linear extension

X-radiographs of sliced samples were produced using a methodology modified from Helmle et al. (2011). Slices were placed on Kodak Industrex film 1.5 m away from an X-ray source set to 70 kV and 15 mA, and were exposed for 10 s. A medical X-ray scanner was then used to digitize manually developed X-ray film negatives. Density bands were not always visible because of the high bulk skeletal density of the samples. Comparable observations were made by Baker & Weber (1975) for coral collected at similar depths. Therefore, the procedures that follow were performed on the 5 slices (each from a different coral colony) from each site with the clearest banding.

Lines were traced over corallite high-density bands (using Adobe Photoshop) where the largest number of repetitive bands could be identified. The distance between adjacent bands was assumed to represent 1 annual cycle (Hubbard & Scaturo 1985), as verified for shallow Florida Keys *Orbicella annularis* coral colonies (Hudson et al. 1976). Tracing continuous density bands between neighboring corallites was not possible because of the high luminance contrast between coenosteums and corallites (Fig. 2a).

The extension/luminance mode of Coral X-Radiograph Densitometry System (CoralXDS; Helmle et al. 2002) was used to measure coral extension rates. Rectangular transects less than 1 corallite thick and oriented parallel to the growth axis were selected on digitized X-ray images where density bands had previously been mapped. On each slice, 3 to 5 adjacent corallite transect scans were conducted. For each transect, pixels from the digitized X-rays were converted into grayscale luminance values (0 to 255) and averaged over the transect width to plot luminance data along the length of the transect (Fig. 2a). The high- and low-density bands were delimited based on a combination of the 2nd derivative zero crossing of the luminance data and the half range value between adjacent peaks and valleys, as in Helmle et al. (2011). Two individual transect luminance plots adjacent to sample locations for isotopic analysis were imported into the program Plot Digitizer to identify periodicity of luminance intervals comparable with isotope sampling intervals.

Selected band boundaries from each transect were plotted on the digitized X-radiograph, compared directly with previous visual estimates, and associated with high-density bands from adjacent corallite transects (Fig. 2b). Density band measurements from each corallite per slice were averaged for each band from adjacent corallites to determine the slice extension length for each year. The mean of all annual extension rates for slices from the same coral sample were then calculated to obtain the sample average

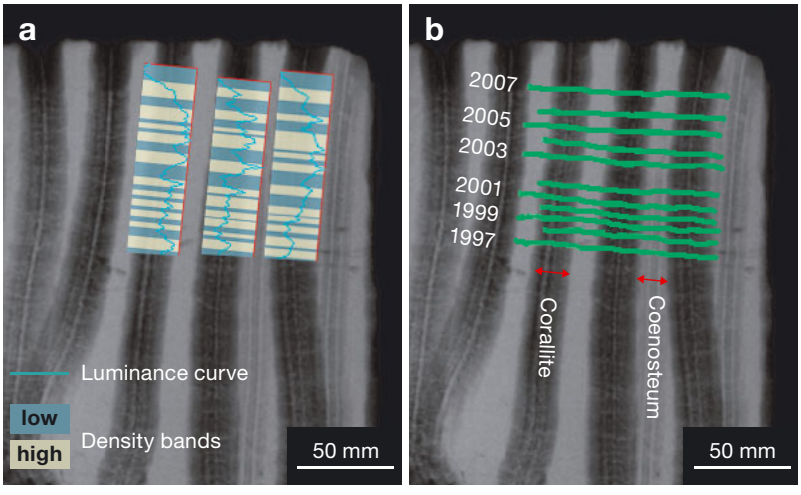

Fig. 2. X-ray negative of a platy mesophotic *Orbicella franksi* coral subsample collected from the Deep Flat Basin. X-ray luminance (grayscale) variation differentiates between high (light) and low (dark) density. (a) Scaled CoralXDS (Helmle et al. 2002) luminance scan results plotted atop location of analyzed corallites. (b) Interpretation of connected continuous density bands expressed on adjacent analyzed corallites, with estimated year of formation indicated. The thin slices needed for analysis resulted in the contrasting vertical pattern because corallites are much less dense than their adjacent coenosteums

linear extension rate ($\Delta\overline{LE}$). The distance between the top of the coral and the first identified density band was measured and used with $\Delta\overline{LE}$ to estimate the year each high-density band was formed, assuming the top of each X-ray slice represents September 2011 (when the samples were collected). Linear extension rates per assumed year were plotted simultaneously per site. Significant differences between mean site linear extension rates were tested using 1-way ANOVA. Post hoc multiple comparisons of means were carried out with Tukey's HSD test.

Skeleton bulk density and calcification

A modified buoyant weight technique was used to obtain the bulk density of analyzed samples (Spencer Davies 1989, Bucher et al. 1998, Smith et al. 2007). To eliminate the effect of bioerosion and secondary accretion on measurements of pure skeletal density, the bottoms of the slices where this activity was observed were cut off and not included for the buoyant weight technique. This also helped to make the length and the corresponding sample density measurements comparable to the transect lengths used to obtain linear growth rates. More slices and samples were used to measure density than to obtain linear extension rates because the buoyant weight technique was not limited by the clarity of density bands, allowing for more accurate representative average density calculations. The X-radiography and gamma densitometry methodology suggested by CoralXDS and others (Chalker & Barnes 1990, Helmle et al. 2002) was deemed to be a less appropriate method to measure the bulk density of samples, because the slabs needed to be cut very thin to reveal the banding, and these methods rely on averaging over the thickness of the slab.

Slices were first placed on a scale to measure dry weight (DW_{clean}). To form a water-tight barrier, slices were immersed in molten paraffin wax (set at 110°C; Smith et al. 2007). Once dry, wax-coated samples were reweighed (DW_{wax}). The buoyant weight (BW_{wax}) of each waxed slice was measured in an enclosed tub of seawater while temperature and salinity were measured simultaneously and used to calculate the tub seawater density (ρ_s) for each slice (Millero & Huang 2009). The following equations (Bucher et al. 1998) were then used to calculate the total enclosed volume ($V_{enclosed}$) and slice bulk density (BD):

$$V_{enclosed} = (DW_{wax} - BW_{wax}) \times \rho_s$$
$$BD = DW_{clean} / V_{enclosed} \quad (1)$$

Different slice bulk density measurements from the same coral sample were averaged to determine the sample average bulk density. Slice average linear extension rates were then multiplied by average bulk density values from the same sample the slice came from to obtain the sample average calcification rate ($\Delta\overline{C}$). Bulk density measurements were not possible for 2 samples (DFB.1 and DFB.10 broke prior to density measurements), so the site average bulk density ($\overline{BD}$) was used as an estimate to obtain calcification rates for these samples. Identification of differences between sites and subsequent multiple pairwise comparisons were determined with 1-way ANOVA and Tukey's HSD testing, respectively.

Stable isotopic analysis

One random representative slice was selected from each of the 3 sites (samples DFB.4, PB.9, SB.7) for stable isotope analysis (SIA). Samples were drilled every 50 µm along the thecal wall, parallel to adjacent luminance transect locations. Using a low-speed microdrill with a 0.5 mm diamond drill bit and a plunge depth of 50 µm, 5 to 8 drill passes were made to collect enough material for SIA. Drilling began 7 to 8 mm from the top of the most recent living coral growth horizon, with subsequent drilling conducted incrementally upward to the most recent living surface of the coral. Samples were dissolved with phosphoric acid and analyzed for $\delta^{13}C$ and $\delta^{18}O$ with an automated carbonate device (Kiel II) connected to a Delta Plus mass spectrometer at the University of Miami Stable Isotope Laboratory. Precision and accuracy, calculated from standards run along with samples, were 0.07 and 0.06‰, respectively, for $\delta^{13}C$ (n = 96), and 0.14 and 0.13‰ for $\delta^{18}O$ (n = 95).

To track the degree of coherence between stable isotope data ($\delta^{13}C$ and $\delta^{18}O$) and luminance values as a function of distance along the transects, wavelet semblance analyses were performed using the continuous wavelet transform (CWT) method (Cooper & Cowan 2008) and a modified MATLAB script. To identify the major periodicities and/or wavelets along the transects, each data set was decomposed into its major components using the complete ensemble empirical mode decomposition (CEEMD) approach (Torres et al. 2011). Subsequently, wavelet power spectrum analyses were performed on each individual component using the Morlet wave (Torrence & Compo 1998) and a modified MATLAB script. Notable periodicities and/or wavelets with global power spectra >1σ confidence level were con-

sidered significant according to the wavelet power spectra of each component. Only components with significant periodicities and/or wavelets were demonstrated. Prior to the analysis, each data set was detrended and linearly interpolated at a constant 0.05 mm, which closely approximates the average sampling resolution for luminance and isotope data. Isotopic compositions from the Primary Bank site were also compared to sea bottom temperatures (1 m above surface), recorded from May to December 2008 with Acoustic Doppler Current Profilers (ADCPs) by the USVI Territorial Coral Reef Monitoring Program (TCRMP) (Smith et al. 2010).

Bioerosion, secondary accretion, and total framework growth

To determine the spatial area of carbonate removed by bioerosion and added by secondary accretion (Fig. 3), 2 non-adjacent slices from 7 to 8 samples per site were analyzed using a modified point count analysis (Macdonald & Perry 2003, Weinstein et al. 2014). Dry slices were scanned to produce unaltered 2-dimensional digital image projections. Multiple slices for each sample were used to increase measurement accuracy. Using the program Coral Point Count with Excel Extension v. 3.6 (Kohler & Gill 2006), a minimum of 300 points (a sufficient number of points according to rarefaction curve analysis) were randomly distributed on each digitized slice and were identified as framework, macroborings, or secondary accretions.

The percentage area of macroboring and secondary accretion was calculated as the sum of macroboring points or secondary accretion points, divided by the sum of macroboring and framework points. Results from each sample pair were averaged to determine the sample mean for each parameter. The sample mean percent area of macroboring and secondary accretion were multiplied by the associated sample $\Delta\overline{C}$ (when available) or the overall site average $\Delta\overline{C}$, calculated only from samples where direct linear extension calculations were provided. This method provides a minimum macroboring and secondary accretion rate because the substrate modification processes are assumed to be at a constant rate, regardless of the amount of substrate available. For example, if a coral grew for 3 yr without any erosion, followed by 3 yr with constant macroboring activity, followed by 3 yr with a macroboring hiatus, the rate of change for macroboring carbonate removal reported using the described technique provides the percentage macroboring divided by 9 yr, not 3 yr, resulting in a smaller value.

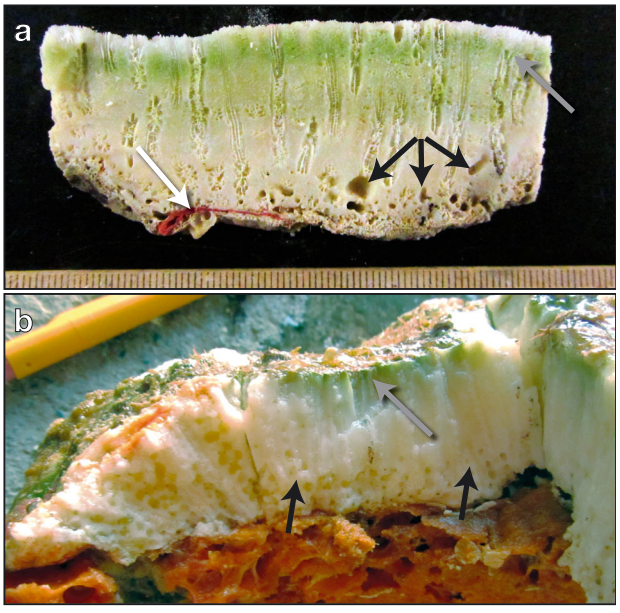

Fig. 3. Mesophotic reef framework bioerosion and secondary accretion. (a) Sample from *Orbicella franksi* colony collected from the Deep Flat Basin. Black arrows show examples of 'living framework' macroboring and white arrow provides an example of living framework secondary carbonate accretion, all on the lower side of the coral. (b) Different collected mesophotic *O. franksi* sample with bioeroding sponge still attached to the underside of the colony, where no protective coral tissue cover was present. Above the sponge, tiny eroded chambers are observed within the coral skeleton (black arrows, for example). Gray arrows in both images identify microboring cyanobacteria community of *Ostreobium* spp.

To determine the overall production accumulation of framework *O. franksi* carbonate, primary coral growth and framework bio-modification was compared. The calculated bioaccretion rates and the negative macroboring rates were added to the previously calculated framework calcification rates obtained from the same sample. Site average bioaccretion and macroboring rates were used for 1 sample (DFB.10) that was destroyed prior to point count analysis. A statistical comparison between overall macroboring versus secondary accretion rates of all sites was calculated with Welch's 2-sample *t*-test. Per site, macroboring and secondary accretion rates were not normally distributed, so testing for significant differences was made with a 1-way Kruskal-Wallis non-parametric comparison. However, when combining all rates, data were found to have normal distributions so 1-way ANOVA and Tukey's HSD were used to test for significant differences between site average framework growth rates. All statistical analyses for this study were conducted with R v. 3.0.3 (R Core Team 2014).

RESULTS

Mesophotic reef coral growth

Measurements for all samples are displayed in Table 1. Average linear extension at 3 different upper mesophotic coral reef habitats in the northern USVI fit standard models of decreasing *Orbicella* spp. coral growth rates with depth (Fig. 4a) (Bosscher & Meesters 1993, Hubbard 2009). Linear extension rates measured in this study were also lower than most rates recorded for orbicellids by previous studies between 25 and 50 m depth (Fig. 4b) (Baker & Weber 1975, Dustan 1975, Hubbard & Scaturo 1985, Huston 1985, Bosscher & Meesters 1993). The average linear extension rate of all mesophotic coral samples measured in this study was 0.80 ± 0.03 mm yr^{-1} (±SE). Between sites, average linear extension rates were significantly different, as indicated by 1-way ANOVA ($F_{2,12}$ = 10.48, p = 0.002). Significant site differences were also found among average calcification rates ($F_{2,12}$ = 7.49, p = 0.008). However, pairwise analysis only found significant differences between the Primary and Secondary Bank sites ($\Delta\overline{LE}$: p = 0.002; $\Delta\overline{C}$: p = 0.007). The fastest $\Delta\overline{LE}$ and $\Delta\overline{C}$ rates occurred at the Secondary Bank, the shallowest

Table 1. Bulk density, linear extension rates, calcification rates, framework bio-modification rates (macroboring and secondary accretion), and total framework growth rates per sample and site averages. Total framework growth rate was only calculated if the linear extension rate for that sample was measured. *Italic*: site average bulk density or site average linear extension rate was used for calculation; underlined: samples used for isotopic analysis; na: data not available. Average values for each site were obtained by taking the mean from each sample, not by multiplying site average values (like density times linear extension). Values are reported with ±1 SE

Sample	Average density ($g\ cm^{-3}$) (no. of slices)	Average linear extension rate ($mm\ yr^{-1}$) (no. of years)	Calcification rate ($kg\ m^{-2}\ yr^{-1}$)	Framework macroboring rate ($kg\ m^{-2}\ yr^{-1}$)	Framework secondary accretion rate ($kg\ m^{-2}\ yr^{-1}$)	Total framework growth rate ($kg\ m^{-2}\ yr^{-1}$)
Deep Flat Basin						
DFB.1	na	0.826 ± 0.066 (7)	*1.701 ± 0.139*	0.165 ± 0.055	0.000 ± 0.000	*1.535 ± 0.150*
DFB.2	2.011 ± 0.020 (3)	na	na	*0.181 ± 0.062*	*0.024 ± 0.018*	na
DFB.4	2.106 ± 0.037 (1[a])	0.813 ± 0.045 (14)	1.711 ± 0.099	0.157 ± 0.053	0.000 ± 0.000	1.554 ± 0.112
DFB.5	1.899 ± 0.061 (2)	na	na	*0.188 ± 0.051*	*0.046 ± 0.046*	na
DFB.6	2.050 ± 0.008 (3)	0.780 ± 0.083 (7)	1.599 ± 0.170	0.364 ± 0.053	0.104 ± 0.022	1.340 ± 0.180
DFB.7	2.016 ± 0.031 (4)	na	na	*0.669 ± 0.033*	*0.027 ± 0.005*	na
DFB.8	2.144 ± 0.072 (3)	na	na	*0.657 ± 0.041*	*0.015 ± 0.007*	na
DFB.9	2.196 ± 0.031 (3)	0.863 ± 0.082 (12)	1.895 ± 0.181	0.126 ± 0.018	0.000 ± 0.000	1.769 ± 0.182
DFB.10	na	0.730 ± 0.056 (8)	*1.503 ± 0.118*	na	na	*1.217 ± 0.144*[b]
Average	**2.060 ± 0.037**	**0.802 ± 0.022**	**1.682 ± 0.065**	**0.313 ± 0.080**	**0.027 ± 0.012**	**1.483 ± 0.095**
Primary Bank						
PB.3	2.001 ± 0.020 (3)	0.571 ± 0.019 (16)	1.143 ± 0.040	0.037 ± 0.003	0.000 ± 0.000	1.106 ± 0.040
PB.7	2.104 ± 0.047 (3)	0.654 ± 0.039 (9)	1.376 ± 0.088	0.243 ± 0.032	0.000 ± 0.000	1.133 ± 0.093
PB.9	1.922 ± 0.040 (3)	0.816 ± 0.051 (12)	1.568 ± 0.103	0.387 ± 0.058	0.005 ± 0.005	1.186 ± 0.119
PB.10	2.198 ± 0.144 (3)	0.749 ± 0.093 (6)	1.647 ± 0.231	0.433 ± 0.141	0.000 ± 0.000	1.214 ± 0.271
PB.11	2.128 ± 0.057 (1[a])	na	na	*0.131 ± 0.011*	*0.043 ± 0.006*	na
PB.12	2.033 ± 0.048 (2)	0.679 ± 0.044 (6)	1.380 ± 0.094	0.129 ± 0.017	0.000 ± 0.000	1.251 ± 0.096
PB.13	2.173 ± 0.045 (2)	na	na	*0.367 ± 0.060*	*0.000 ± 0.000*	na
Average	**2.080 ± 0.037**	**0.694 ± 0.042**	**1.423 ± 0.088**	**0.247 ± 0.058**	**0.007 ± 0.006**	**1.178 ± 0.026**
Secondary Bank						
SB.1	2.037 ± 0.015 (3)	na	na	*0.246 ± 0.028*	*0.004 ± 0.004*	na
SB.2	1.966 ± 0.013 (3)	na	na	*0.407 ± 0.019*	*0.012 ± 0.012*	na
SB.4	2.020 ± 0.039 (2)	0.960 ± 0.068 (5)	1.940 ± 0.143	0.270 ± 0.062	0.013 ± 0.013	1.684 ± 0.157
SB.6	2.096 ± 0.025 (3)	0.875 ± 0.037 (13)	1.833 ± 0.080	0.189 ± 0.009	0.000 ± 0.000	1.644 ± 0.081
SB.7	2.004 ± 0.031 (4)	0.859 ± 0.053 (8)	1.722 ± 0.109	0.453 ± 0.040	0.040 ± 0.024	1.309 ± 0.119
SB.8	2.004 ± 0.045 (3)	na	na	*0.302 ± 0.016*	*0.000 ± 0.000*	na
SB.9	1.956 ± 0.086 (2)	0.833 ± 0.060 (5)	1.630 ± 0.137	0.142 ± 0.031	0.139 ± 0.140	1.627 ± 0.198
SB.11	1.945 ± 0.081 (3)	0.979 ± 0.119 (5)	1.904 ± 0.244	0.406 ± 0.052	0.000 ± 0.000	1.498 ± 0.250
Average	**2.004 ± 0.017**	**0.901 ± 0.029**	**1.806 ± 0.058**	**0.302 ± 0.039**	**0.026 ± 0.017**	**1.552 ± 0.068**

[a]Error calculated as the site average SE; [b]Site average framework modification rates used for calculation

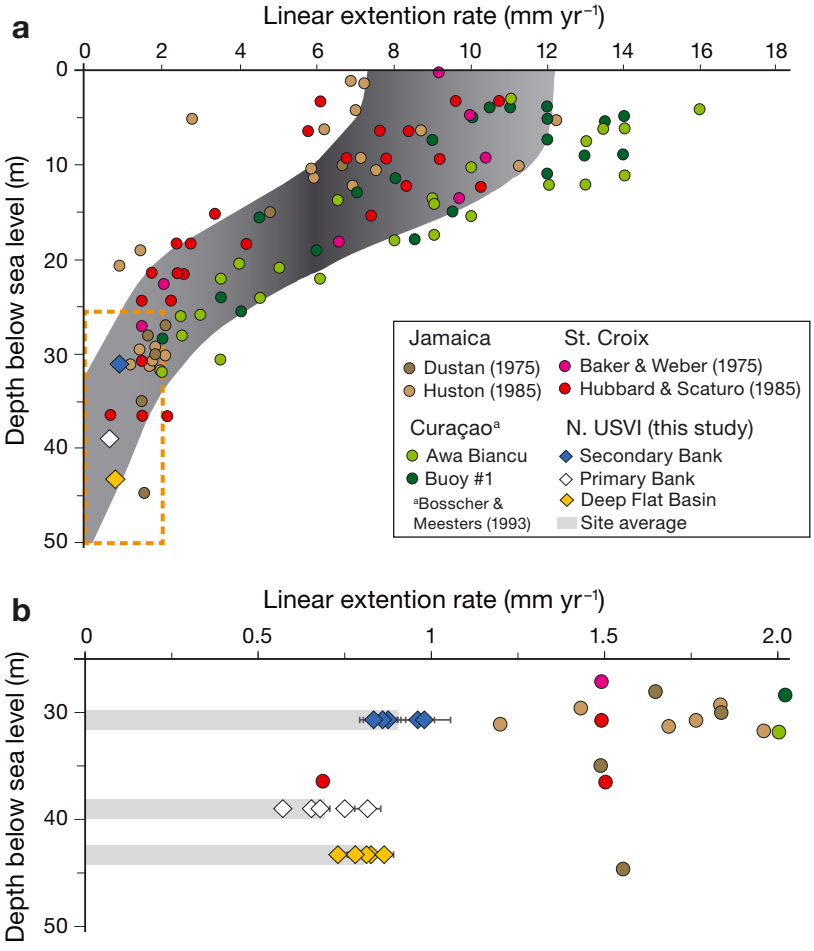

Fig. 4. Linear extension rate versus depth. (a) Comparison of average *Orbicella* spp. linear growth rates measured from this study with other Caribbean measurements (Baker & Weber 1975, Dustan 1975, Hubbard & Scaturo 1985, Huston 1985, Bosscher & Meesters 1993). Shaded area represents predicted range of *Orbicella* spp. growth rates (adapted from Hubbard 2009). Dashed rectangle indicates (b) magnified view of measured growth rates between 25 and 50 m, including rates from every sample analyzed in the current study and site averages (gray bars). Error bars show ±1 SE

mesophotic reef site ($\Delta\overline{LE}$: 0.979 ± 0.119 mm yr^{-1}; $\Delta\overline{C}$: 1.940 ± 0.143 kg m^{-2} yr^{-1}), and the slowest occurred at the Primary Bank ($\Delta\overline{LE}$: 0.571 ± 0.019 mm yr^{-1}; $\Delta\overline{C}$: 1.143 ± 0.040 kg m^{-2} yr^{-1}). The Deep Flat Basin showed intermediate rates between the Bank sites as evident from the site averages (Table 1). Skeleton bulk density was not significantly different between sites ($F_{2,19}$ = 1.702, p = 0.209).

Individual coral sample annual growth rates per site generally experienced similar interannual variation as a function of time (Fig. 5). Irrespective of differences in means, interannual variability can be described by the coefficient of variation (standard deviation divided by the mean; Helmle et al. 2011). The average coefficient of variation for extension rates were 24.9, 19.8, and 18.3%, respectively, at the Deep Flat Basin, Primary Bank, and Secondary Bank. These demonstrate a similar amount of interannual variability between sites, results comparable to those obtained from Florida *Orbicella faveolata* cores (Helmle et al. 2011). X-radiographs showed high-density bands that often resembled coral dissepiments in size and position. These images were consistent with previous studies that have shown that the annual density variations recorded in the coral genus *Orbicella* are directly associated, to some extent, with dissepiment thickening (Dodge et al. 1993, Dávalos-Dehullu et al. 2008).

Luminance and stable isotopic comparison

Previous studies show that carbon and oxygen stable isotope trends from coral skeletons display an annual periodicity (Fairbanks & Dodge 1979, Swart et al. 1996). As such, the cyclical coral stable oxygen and carbon isotopic composition curves identified in 3 representative samples provide a coarse verification of the annual density band formation assumption, independent from the X-radiographic methodology. A direct correlation between skeletal $\delta^{13}C$ and $\delta^{18}O$ values was seen for the 3 sites (Fig. S1a in the Supplement at www.int-res.com/articles/suppl/m559p045_supp.pdf). Additionally, a direct inverse correlation between $\delta^{13}C$ and luminance values was seen in the Secondary Bank sample, but no similar correlation was observed from the Primary Bank and the Deep Flat Basin (Fig. S1a).

Since the $\delta^{13}C$, $\delta^{18}O$, and luminance time series in nature may contain unsuspected correlations or may present variable correlations through time (Sharifi et al. 2015), we used wavelet spectral analysis to identify if the potential correlation among them is sustained throughout the entire record. Results of CWT analysis and corresponding semblance analysis conducted on $\delta^{13}C$ and coral skeletal luminance data sets from each site are displayed in Fig. 6. Spatial correlation between luminance and stable isotopic values for each

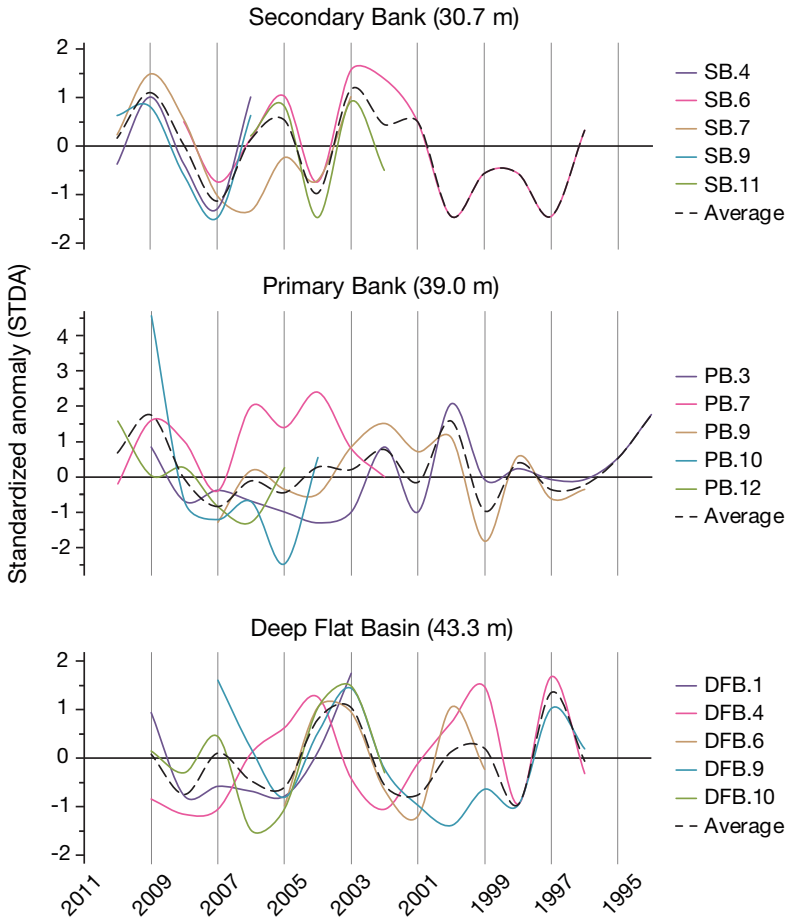

Fig. 5. Standardized anomaly (STDA) in linear extension rate variation with time. Curve colors correspond to specific sample results at a given site. Dotted black lines are overall site averages. STDA is the annual deviation from the mean (yearly average minus average of all years), divided by the standard deviation of all years

sample analyzed is provided in Table S1 & Fig. S2 in the Supplement. The semblance analysis indicated a significant negative correlation (–1) between $\delta^{13}C$ and luminance values for the samples from the Secondary and Primary Banks (Fig. 6a,b). Contrary to these 2 sites, the semblance analysis revealed a strong positive correlation (+1) between $\delta^{13}C$ and luminance values for the sample from the Deep Flat Basin (Fig. 6c). Wavelet power spectrum analysis conducted on major components of the $\delta^{13}C$, $\delta^{18}O$, and luminance data sets from each site revealed several significant wavelets (global power spectrum above 1σ). These wavelets were indicative of cyclic changes in $\delta^{13}C$, $\delta^{18}O$, and luminance values along the growth axis and were centered at 0.45 to 0.75 mm, 0.9 to 1.2 mm, 1.5 to 1.9 mm, and 2.3 to 2.8 mm (Fig. S1 in the Supplement). The common wavelets between all 3 variables ($\delta^{13}C$, $\delta^{18}O$, and luminance) at the 3 study sites were centered at 1.5 to 1.9 mm (Fig. 7). Additionally, samples from the Primary and Secondary Banks shared another wavelet centered at 0.45 to 0.75 mm. Wavelet power spectrum analysis also revealed that the $\delta^{18}O$ values at the Secondary Bank vary at higher frequencies (from 0.5 to 1.8 mm), while the lowest frequencies in $\delta^{18}O$ are recorded at the Deep Flat Basin (from 1.0 to 1.9 mm). For $\delta^{13}C$, the highest frequency variations were recorded at the Primary Bank (from 0.5 to 1.2 mm) and the lowest frequency variations were recorded at the Secondary Bank (from 1.6 to 2.4 mm).

Variation in $\delta^{13}C$, $\delta^{18}O$, and luminance (representing skeletal linear extension) as a function of sea bottom temperature from May to December 2008 at the Primary Bank site is shown in Fig. 8. Higher luminance and more depleted $\delta^{13}C$ and $\delta^{18}O$ values were correlated with warmer temperatures. Correlation between luminance and $\delta^{13}C$ with sea bottom temperature appeared more pronounced than between $\delta^{18}O$ and sea bottom temperature. Variation in $\delta^{13}C$ and $\delta^{18}O$ values with respect to depth are shown in Fig. 9. The average $\delta^{18}O$ values showed almost no variation with respect to depth (Secondary Bank: $\delta^{18}O_{ave.}$ = –3.85‰; Primary Bank: $\delta^{18}O_{ave.}$ = –3.73‰; Deep Flat Basin: $\delta^{18}O_{ave.}$ = –3.64‰). In contrast, the average $\delta^{13}C$ values for each site were different (Secondary Bank: $\delta^{13}C_{ave.}$ = –2.02‰; Primary Bank: $\delta^{13}C_{ave.}$ = –2.24‰; Deep Flat Basin: $\delta^{13}C_{ave.}$ = –1.23‰) and do not follow a depth profile, since the most depleted $\delta^{13}C$ value was recorded at the Primary Bank. The highest range in $\delta^{13}C$ and $\delta^{18}O$ values was also recorded at the Primary Bank.

The results of wavelet analysis conducted on a 12 yr long luminance time series from the Primary Bank indicated a 1.4 to 2.0 yr periodicity. This is in good agreement with the periodicities of the SOI (1.6 to 2.7 yr) (Fig. S3 in the Supplement) as an indicator of warm and cold (El Niño and La Niña) periods in ocean surface temperature (Ropelewski & Jones 1987).

Framework macroboring and secondary accretion

For overall living framework bio-modification, Welch's 2-sample *t*-test indicated that rates of *Orbicella franksi* skeleton macroboring carbonate re-

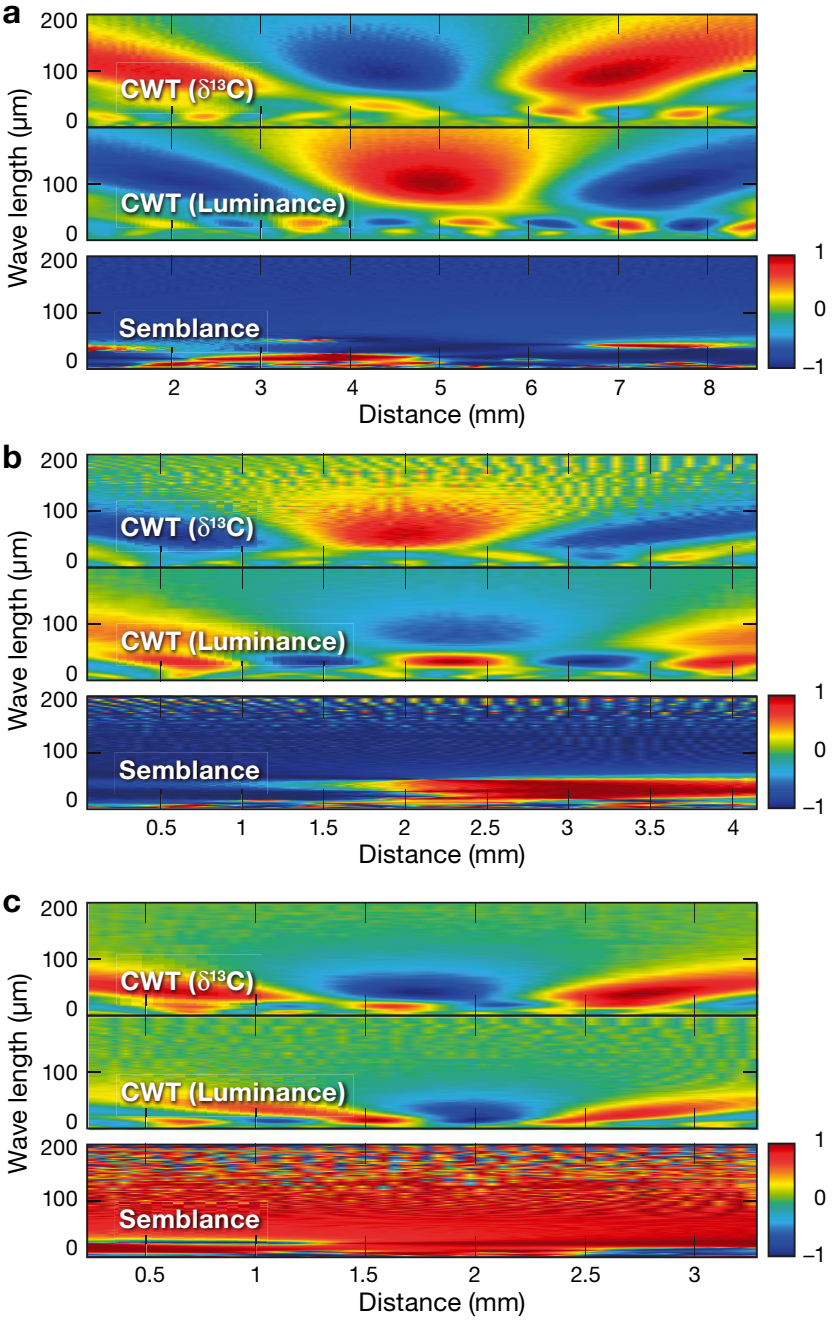

Fig. 6. Variation of $\delta^{13}C$ with respect to luminance for samples from (a) the Secondary Bank, (b) the Primary Bank, and (c) the Deep Flat Basin. Cross-wavelet transform (CWT) for each $\delta^{13}C$-luminance pair and their corresponding semblance wavelet analysis capture covariations of isotopic and luminance values as a function of distance (mm) in each sample along the analyzed transect. Red areas in CWT panels indicate positive amplitude and dark blue indicates negative amplitude. The degree of correlation between relative abundances of $\delta^{13}C$-luminance pairs in the panels referring to semblance analysis is shown in red, corresponding to a semblance of +1 (positive correlation), green to a semblance of zero, and dark blue to a semblance of –1 (negative or inverse correlation). The $\delta^{13}C$ and luminance show a significant negative correlation (–1) for most of the record for samples from the Primary and Secondary Banks. Strong positive correlation (+1) existed between $\delta^{13}C$ and luminance in the sample from the Deep Flat Basin

moval were significantly faster than rates of secondary carbonate accretion (t_{23} = 7.58, p < 0.001), but that both were slow compared with primary coral framework calcification (Fig. 10). Average framework *O. franksi* macroboring and secondary accretion rates were lowest at the Primary Bank (Table 1). However, no significant differences were found in framework macroboring rates (df = 2, χ^2 = 1.19, p = 0.557) or secondary accretion rates (df = 2, χ^2 = 2.39, p = 0.302) between the 3 sites. Average percent of macroboring and secondary accretion cover per sample is provided in Table S2 in the Supplement.

Total framework growth

The unit area net rate of carbonate production directly contributing to framework growth of living mesophotic coral reefs can be understood when comparing the 2 carbonate framework accretion processes (primary calcification and secondary accretion) with macroboring (Fig. 10). Analysis showed that the average summation of framework growth is significantly different between mesophotic coral reef habitats ($F_{2,12}$ = 8.26, p = 0.006). Post hoc comparisons indicated specific framework growth (calcification) rate differences between samples from the Primary Bank site and samples from both the Secondary Bank (p_{adj} = 0.006) and the Deep Flat Basin (p_{adj} = 0.023). Average sample and site linear extension rates, bulk density, calcification rates, framework bio-modification rates (macroboring and secondary accretion), and total *O. franksi* framework growth rates are presented in Table 1.

Grazing was assumed to remove minimal quantities of carbonate from living coral framework samples collected on northern USVI mesophotic coral reefs. Few grazing organisms are believed to remove distinguishable amounts of carbonate from living

coral colonies (Randall 1974, Bruggemann et al. 1996). Examination of the living surface of collected samples in the USVI indicated no major signs of parrotfish coral-livory that would remove underlining skeleton, and no clear indicators of parrotfish grazing (such as typical grazing scars) were observed on the non-living outer surfaces. Green bands indicative of the microboring cyanobacteria *Ostreobium* spp. were found on some slices (Fig. 3, gray arrows). Although microboring rates for dead substrate at 30 m in the Caribbean have been determined (Vogel et al. 2000), living coral have different euendolithic microorganism communities (Le Campion-Alsumard et al. 1995), for which it is difficult to measure direct bioerosion rates. Microboring was still partially factored into overall total framework growth calculations by accounting for differences in weight from microboring when measuring bulk density with the buoyant weight technique. However, we were unable to distinguish between direct differences in weight from coral density variation and microboring carbonate removal.

DISCUSSION

Results from this study provide new data on coral growth rate variability at neighboring mesophotic coral reefs with differ-

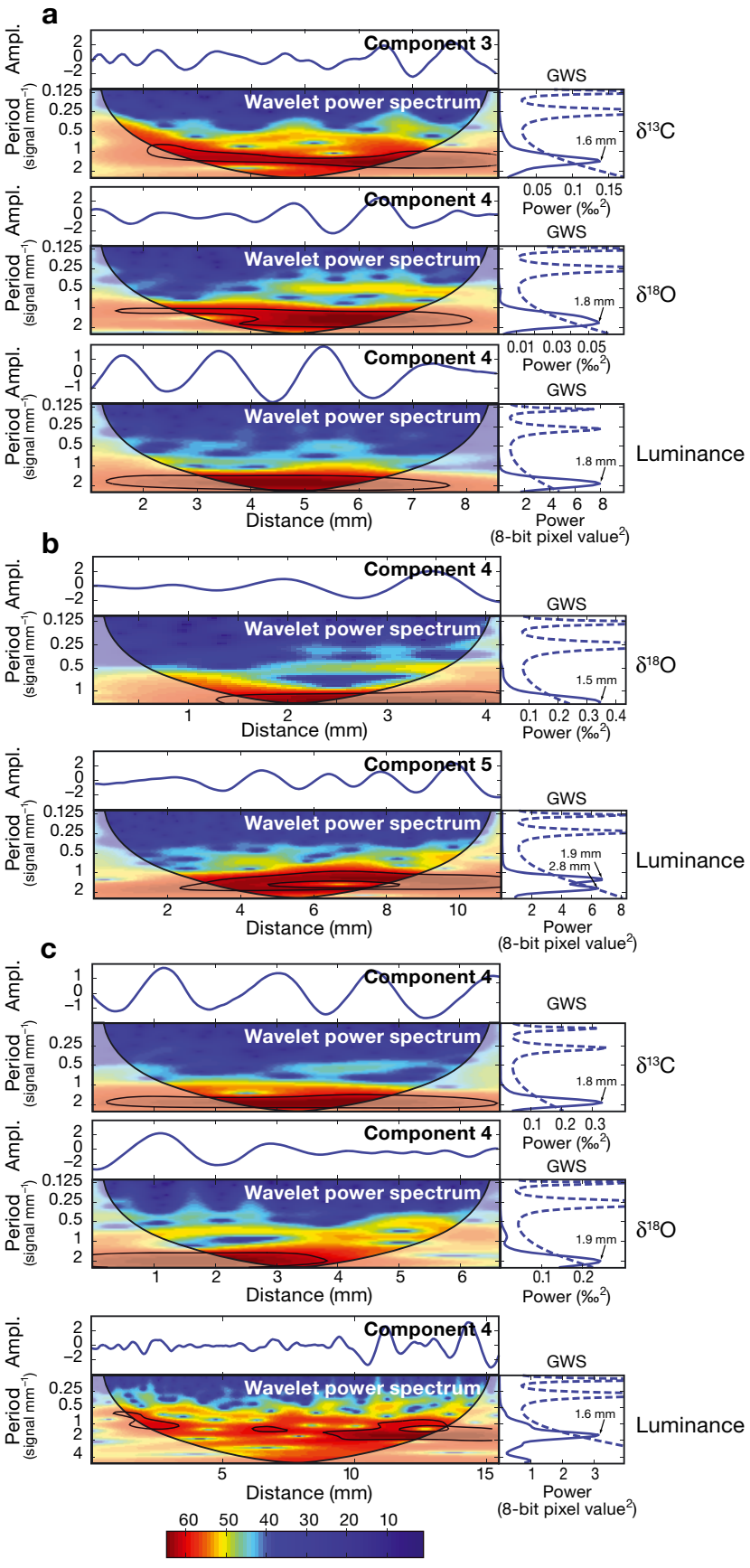

Fig. 7. Wavelet power spectrum of the major components of detrended $\delta^{13}C$, $\delta^{18}O$, and luminance data sets for samples from (a) the Secondary Bank, (b) the Primary Bank, and (c) the Deep Flat Basin. Units for amplitude are the same as the units of the original variables (‰ for isotope data and 8-bit color value for the luminance). Faint-colored areas denote the cone of influence (Torrence & Compo 1998) and black enclosed dark red boundaries mark 1σ confidence level. The most significant peaks of spectral power are shown on the global power spectrum (GWS) panels. Dashed lines refer to 1σ confidence level. A valid signal is observed when the solid line in a GWS panel is above the confidence interval (dashed line). The color bar at the bottom refers to the wavelet power values from dark blue (low values), to dark red (high values). Period unit: Signal appearance as a function of distance (see 'Materials and methods — Stable isotope analysis'). Ampl.: amplitude

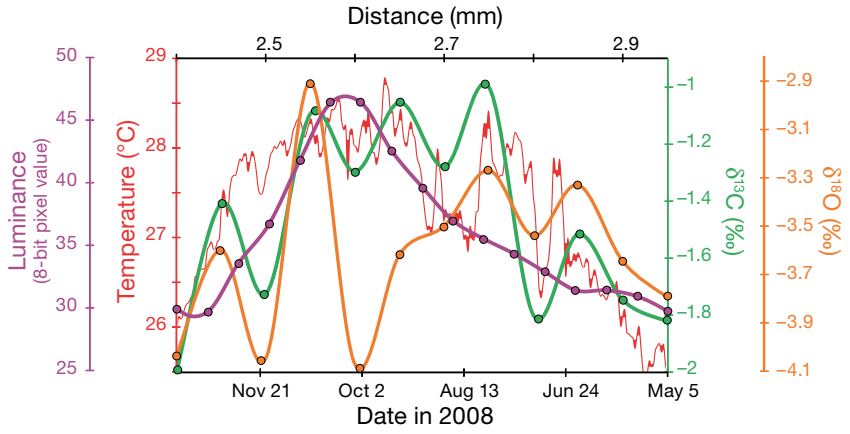

Fig. 8. Variation of $\delta^{13}C$, $\delta^{18}O$, and luminance with respect to changes in sea bottom temperature recorded at the Primary Bank site from May to December 2008. Luminance values are based on pixel brightness 8-bit integer representation scale ranging from 0–255 (with 255 taken as white)

ent geomorphological properties on a low-angle insular carbonate shelf. These results are assumed to be an accurate representation of recent linear growth rates, even though average linear extension rates were calculated using slightly different time intervals for different samples. Linear extension rate averages per sample were measured from different time periods between 1994 and 2010, based on the ability to resolve density bands from very thin slices. However, density bands were resolvable from at least 3 of the 5 samples per site between 2003 and 2009. When only including these samples from the same time interval, site average linear extension rates were found to have similar values and interannual variations between sites (Secondary Bank: 0.91 ± 0.05 mm yr^{-1}; Primary Bank: 0.68 ± 0.02 mm yr^{-1}; Deep Flat Basin: 0.82 ± 0.04 mm yr^{-1}) as when all available data were averaged (Table 1). Stabilization to more consistent averages as more sampling years are added justify using the maximum amount of recovered data, increasing the ability to detect significant differences.

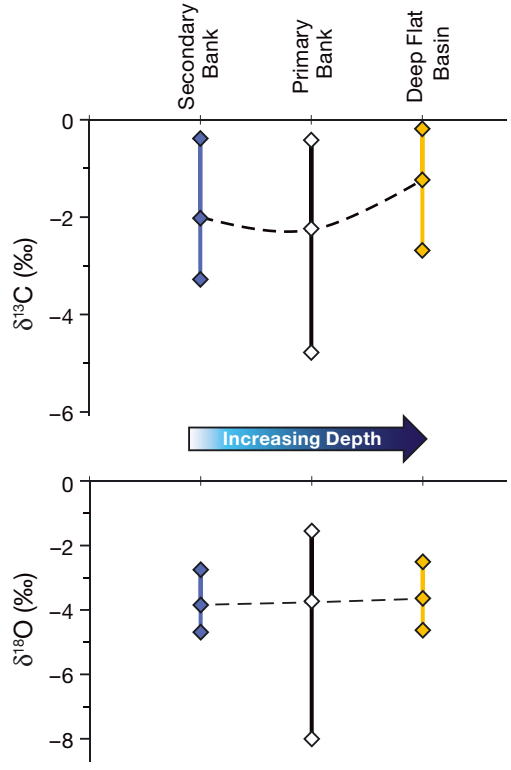

Fig. 9. Variation of $\delta^{13}C$ and $\delta^{18}O$ with respect to depth at each site. The vertical solid lines indicate the range of $\delta^{13}C$ and $\delta^{18}O$ recorded at each site and the outermost points (◆) indicate the maximum and minimum values. The points in the middle indicate the average values and the dashed black line shows the trend of average $\delta^{13}C$ and $\delta^{18}O$ between sites

Slow growth

As shown in previous studies, upper mesophotic coral reef *Orbicella franksi* growth rates were found to be slower than rates calculated for the same coral at shallower depths in the USVI and Puerto Rico (Baker & Weber 1975, Gladfelter et al. 1978, Hubbard & Scaturo 1985, Torres & Morelock 2002). This large-scale difference is mostly attributable to decreasing irradiance with depth (Bosscher & Meesters 1993, Lesser et al. 2010). The decline of growth rates in this region might also be attributed to a documented reduction in calorimetric energy, lower temperatures, and greater short-term thermal variability compared to shallower locations (Brandtneris et al. 2016). Additionally, the majority of depth-generalist Caribbean coral species, including *O. franksi* (Rowan & Knowlton 1995), have been shown to host distinct depth zonations of *Symbiodinium* (see data compilation by Bongaerts et al. 2010). Differences in *Symbiodinium* assemblage and diversity can impact multiple indicators of coral growth and calcification (Little et al. 2004, Jones & Berkelmans 2010, Pettay et al. 2015), but more research is needed to determine if *Symbiodinium* depth zonation in orbicellids is another major factor for decreased coral growth rates in mesophotic reefs.

The abundance of phytoplankton is also known to impact coral growth rates (see review by Houlbrèque

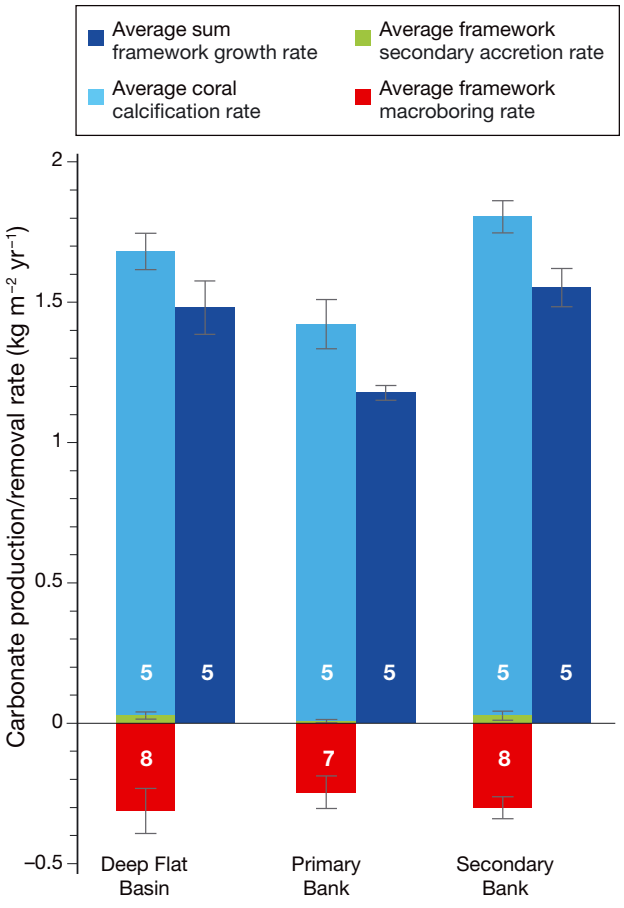

Fig. 10. Mesophotic reef *Orbicella franksi* framework calcification and bio-modification rates (macroboring and secondary accretion), and total average *O. franksi* framework growth rates. Number of samples used for each calculation (values in bars) are the same for macroboring and secondary accretion. Average framework growth and calcification rates were only calculated from samples where linear extension was measured directly. See Table 1 for reported average framework secondary accretion and macroboring rates. Error bars show ±1 SE

& Ferrier-Pagès 2009). Phytoplankton concentrations can be higher in upper MCEs during the warm season, when stratification brings the first thermocline to 30 to 50 m depth (Lesser et al. 2010) and the zone of the seasonal chlorophyll maximum layer to our study sites (Smith et al. 2010, 2016b). Although this represents a potential heterotrophic food source to offset autotrophic energy lost from decreasing PAR (Leichter & Genovese 2006), the caloric content of orbicellid corals drops in the warm season, potentially tied to reproduction (Brandtneris et al. 2016). It is clear that this exogenous food supply is not able to offset declined growth with depth.

Despite slower growth rates, modern *O. franksi* coral cover at the Primary and Secondary Bank sites has been shown to be higher than at shallower reef locations for the past 3 decades in the same region (Armstrong et al. 2006, Smith et al. 2013, 2016b). This indicates that locations with some of the highest coral cover in the USVI have some of the slowest coral growth rates. Similar observations were made at shallow (1 to 5 m) nearshore Cape Verde Islands *Siderastrea radians* reefs off the west coast of Africa (Moses et al. 2003). Results from the USVI imply that orbicellids do not require fast growth rates to become the dominant framework builders of mesophotic coral reef habitats. One likely reason for this could be that bioerosion rates tend to be lower in mesophotic coral reefs (Weinstein et al. 2014), such that even slow growth rates are sufficient to allow carbonate accretion and the formation of complex habitats (Hubbard 2009). Slower bioerosion could also lead to high rates of substrate colonization by coral larva and less competition for space with bioeroding organisms. Another possibility is that although linear extension rates were slow, calcification rates were higher because of the high bulk density measured in collected samples. This may suggest that *O. franksi* has a large tolerance for slowing growth rates by increasing its density, allowing it to persist even at what appears to be the depth limits of its habitat range. From an environmental perspective, some gently sloping upper MCEs may also be partially buffered from storm and swell disturbances (Goldberg 1983, Bongaerts et al. 2010), which act as major controlling factors of orbicellid reef formation in shallower depths (Chollett & Mumby 2012). Although some low-angle mesophotic reefs are not completely immune from direct storm disturbances (Bongaerts et al. 2013, White et al. 2013), most storm-related damage to mesophotic reefs occurs on steep slopes and results from indirect effects such as sedimentation, scour, and debris avalanches (see review by Bongaerts et al. 2010). The low frequency of storm impacts on USVI mesophotic reefs, combined with low bioerosion, could lead to stable, slowly accreting reefs that form high coral cover and structural complexity. These features likely have helped lead to sound reef development, despite slow linear growth rates. Alternatively, Smith et al. (2016a) suggested that USVI mesophotic reefs are not immune to storm disturbances but that antecedent geomorphology and associated dislodged colony retention result in the observed high coral cover.

Beyond having slower growth rates than those of shallow water reefs, linear extension rates calculated in our study were among the lowest recorded for orbicellids growing between 30 and 45 m depth (Baker & Weber 1975, Dustan 1975, Hubbard & Scaturo 1985,

Huston 1985, Bosscher & Meesters 1993). This result was not attributable to differences in technique, as the majority of previously conducted studies comparable to our current analysis used very similar X-radiography methodology and a similar number of samples per location (Baker & Weber 1975, Hubbard & Scaturo 1985, Huston 1985, Bosscher & Meesters 1993). One potential reason for the slower rates in our study is that different *Orbicella* spp. morphotypes have been recorded with different growth rates at the same depth; growth rates for *O. franksi* are generally slower than those of *Orbicella annularis* (Tomascik 1990, Van Veghel & Bosscher 1995). Although we measured *O. franksi* growth rates in the USVI, it is unknown which members of the *Orbicella annularis* species complex were measured by comparative studies (Baker & Weber 1975, Dustan 1975, Hubbard & Scaturo 1985, Huston 1985, Bosscher & Meesters 1993). However, as most of those corals were described with platy, 'flattened' morphologies, we suspect similar morphotypes and species were used for our comparison to these other studies.

Another possible explanation for the differences in growth rates between this study and others at similar depths might be that environmental factors were different 20 to 40 yr earlier. Previous shallower water studies analyzing longer massive coral records or direct measurements of branching coral identified that coral growth rates of the same species have decreased in the past few decades (Guzman et al. 2008, Bak et al. 2009, De'ath et al. 2009, Tanzil et al. 2013). These recorded reductions in growth rate, as well as declines in coral cover, are thought to be related to increasing sea surface temperatures, declining aragonite saturation (ocean acidification), sedimentation and coastal runoff, and volcanic and anthropogenic aerosols (Graham et al. 2006, Hoegh-Guldberg et al. 2007, Kwiatkowski et al. 2013).

A decline in recent linear extension rates of orbicellids in mesophotic coral reef depths may be related to similar global and local factors. Recent work shows that these same orbicellid reef systems in the USVI experienced thermal stress coral bleaching events in 2005 and 2012, likely as a recent response to increasing ocean temperatures and contrary to their hypothesized role as thermal refugia (Smith et al. 2016b). If the growth rate of mesophotic corals is declining, then this would counter previous assumptions that mesophotic reefs are buffered from some of the same environmental disturbances causing the decline of shallower coral reefs (Glynn 1996, Riegl & Piller 2003, Bak et al. 2005, Armstrong et al. 2006). Sea surface temperatures in the Caribbean have been increasing over the past few decades (Sheppard & Rioja-Nieto 2005, Saenger et al. 2009, Chollett et al. 2012), while the Caribbean and North Atlantic sea surface aragonite saturation state levels have continued to decrease (Gledhill et al. 2008, Bates et al. 2012). As USVI mesophotic coral reefs are associated with the surface upper mixed layer of the ocean for part of the year (Smith et al. 2016b), they should also experience some decline in aragonite saturation states. We were unable to directly measure aragonite saturation states at the individual study sites. However, a compilation of measurements in the Northern Atlantic found that aragonite saturation states at 50 m declined from an average of 2.77 between 1989 and June 1998 to 2.74 between June 1998 and 2010 (Jiang et al. 2015).

Another possibility for slower mesophotic coral growth rates than previously recorded is that coral from the northern USVI mesophotic reef system might naturally grow more slowly than in other regions of the Caribbean. However, the local environment of the southeastern Puerto Rican Shelf MCEs indicates exceptional conditions for coral growth, including clear water and current-driven flushing (Smith et al. 2010). In addition, previous studies of USVI mesophotic coral reefs indicate very low sediment trap accumulation rates (Smith et al. 2008), and little terrestrial input and sedimentation that could stunt coral growth rates (Weinstein et al. 2015). Therefore, unless there are biological factors such as genetically determined population-specific growth rates, it seems unlikely that local factors are causing declines in mesophotic coral growth rates compared to earlier studies. Still, *Orbicella faveolata* has been shown to host regional differences in *Symbiodinium* distribution (Kemp et al. 2015), potentially causing unknown regional variability in mesophotic coral growth rates. Future analyses, such as longer age records and a wider spatial sample coverage with *Symbiodinium* analysis, are needed to determine if differences in mesophotic coral growth rates are due to environmental conditions, geographical location, or other unknown factors.

Habitat growth variability

Results from our study provide the first data set of mesophotic coral growth rates from multiple reef habitats/geomorphologies within a region of the Caribbean. Significant, subtle differences were detected in mesophotic reef dominant framework coral linear extension and total calcification rates at relatively

similar depths. Our results also demonstrate the importance of including macroboring and secondary accretion in the overall calculation of total framework calcification rates. These parameters increased the differences among sites that might contribute to total reef framework accretion. When including these parameters, even more variability between sites was discovered. Variations in growth rates between habitats and regions have been found in previous studies (Aller & Dodge 1974, Scoffin et al. 1992, Carricart-Ganivet & Merino 2001). However, another study indicated a lack of growth variability for shallow *O. annularis* found at backreef and forereef habitats in St. Croix, USVI coral (Gladfelter et al. 1978). The drivers of varying coral growth rates between habitats and depths are complex and often interrelated, but are generally caused by differences in predation, depth, light intensity, distance from shore, turbidity, nutrients, and temperature (see review by Pratchett et al. 2015).

Generally, coral stable oxygen isotope variation is influenced by temperature and seawater isotopic composition as a function of numerous properties such as precipitation, salinity, and water mass transport (Carriquiry et al. 1994). Such a relationship can be seen between $\delta^{13}C$, $\delta^{18}O$, and skeletal linear extension (as presented by luminance), with sea bottom temperature variations recorded from May to December 2008 at the Primary Bank site (Fig. 8). However, the $\delta^{18}O$ values show less correlation with more variability compared to $\delta^{13}C$, probably attributed to a greater sensitivity to temperature and salinity fluctuations than to metabolic fractionation (Grottoli & Wellington 1999). Also, the amplitude of the annual variation in sea bottom temperature recorded at the Primary Bank site is too low (ranging from ~25.5 to ~28.5°C) to be able to produce a strong temperature signal in $\delta^{18}O$ values. To further confirm our observations, a longer and continuous record of temperatures is needed for all 3 study sites.

Coral stable carbon isotope composition is influenced by a complicated set of coral–algal metabolic interactions generally thought to act as a 'light meter' (Weber 1974, Swart 1983, Grottoli 1999). Therefore, it is probable that the site-to-site variation in mesophotic *O. franksi* growth parameters is related more to water clarity (and depth) and metabolic differences than to temperature variability. The fastest growth rates were recorded at the Secondary Bank, potentially because this was the shallowest site. However, total *O. franksi* growth rates were slowest at the Primary Bank, which is shallower than the Deep Flat Basin site. Therefore, small depth differences do not appear to be the only driver of mesophotic coral growth rate variability.

Correlations between mesophotic coral skeletal growth variations and stable isotope composition were more readily apparent for $\delta^{13}C$ than $\delta^{18}O$. This is likely attributable to the fact that (1) the annual temperature fluctuations at MCE depths may not vary enough in amplitude to produce strong temperature signals (see temperature data from Smith et al. 2010, Smith et al. 2016b); (2) $\delta^{13}C$ has been shown to have depth-related anomalies such that samples from deeper (15 m instead of 1 m) coral show 2 to 3 times greater amplitude fluctuations in carbonate isotope composition (Carriquiry et al. 1994); and (3) skeletal $\delta^{18}O$ is not metabolically fractionated in corals and shows poor correlation with skeletal extension (Grottoli & Wellington 1999).

For USVI mesophotic coral reefs, coral skeletal extension and $\delta^{13}C$ are correlated at the Primary and Secondary Banks (Fig. 6a,b). However, this correlation becomes somewhat reversed when moving to the deeper Flat Basin site. This may suggest the effect of environmental conditions on coral metabolism (Grottoli & Wellington 1999, Shimamura et al. 2008, Schoepf et al. 2014). The reef sites experience different levels of nutrient input, as shown by variable exposure to phytoplankton abundance (Smith et al. 2010, Smith et al. 2016b), which is known to alter growth rates of other coral species in controlled experiments (Stambler et al. 1991, Atkinson et al. 1995, Ferrier-Pagès et al. 2000). For example, growth rates at the Deep Flat Basin may be faster than those at the Primary Bank because of more heterotrophic food resource availability, as indicated by increased chlorophyll as a possible proxy for zooplankton concentration (Smith et al. 2010).

Skeletal $\delta^{13}C$ values reflect long-term changes in coral metabolism and show depletion with respect to depth (Grottoli 1999, Grottoli & Wellington 1999, Lesser et al. 2010). This depletion trend is somewhat altered at depth (60 m and deeper in the Bahamas) potentially due to equilibrium kinetics (Lesser et al. 2010). A similar trend was observed in the USVI (Fig. 9) where skeletal $\delta^{13}C$ values are depleted from the Secondary Bank ($\delta^{13}C_{ave.}$ = −2.02‰) to the Primary Bank ($\delta^{13}C_{ave.}$ = −2.24‰) and change to less negative values at the Deep Flat Basin ($\delta^{13}C_{ave.}$ = −1.23). This may indicate that despite more heterotrophic food source availability at the Deep Flat Basin (Smith et al. 2010), skeletal $\delta^{13}C$ values are controlled more by equilibrium kinetics than by nutrient availability. In shallower depths, increasing zooplankton abundance has been found to decrease skeletal $\delta^{13}C$ val-

ues and increase growth rates (Felis et al. 1998, Grottoli & Wellington 1999). It is possible that the degree of additional heterotrophic feeding is insufficient to change the isotopic values at the Deep Flat Basin or that the zooplankton/skeletal $\delta^{13}C$ relationship found in shallower water does not counteract the effects of equilibrium kinetics at deeper depths. Future studies are needed to determine how mesophotic reef orbicellid skeletal $\delta^{13}C$ values are affected by changes in zooplankton concentrations, and to obtain more direct measurements of site nutrient differences. Additionally, as dissimilarities in calcification rates could also result from differing levels of aragonite saturation states, future site-specific measurements are needed.

Regardless, cyclic changes detected in mesophotic coral reef $\delta^{13}C$, $\delta^{18}O$ and skeletal growth data are likely a reflection of periodic changes in environmental conditions. The ENSO controls the interaction between the atmosphere and ocean in the Caribbean Sea in a somewhat periodic variation. The cold ENSO phase tends to increase hurricane landfall probabilities relative to neutral or warm phases on interannual and multidecadal timescales (Tartaglione et al. 2003, Klotzbach 2011), and the warm phase results in positive Caribbean rainfall anomalies (Giannini et al. 2000, Giannini et al. 2001). Changes in interannual sea level pressure and sea surface temperature variability associated with Caribbean rainfall are also controlled by ENSO. The agreement between annual variations in skeletal growth and periodic changes in the SOI suggest the potential role ENSO has on influencing growth characteristics of USVI mesophotic coral by controlling water circulation, and as a result, water clarity and nutrient distribution.

Subtle differences in carbonate production provide a long-term mechanism for the creation of heterogeneous reef structure, and maintaining the health and biodiversity of both shallow and deep light-dependent marine coral reef ecosystems confronted by anthropogenic and natural disturbances (Lenihan et al. 2008, McClain & Barry 2010). Therefore, substantial timescale-dependent carbonate accumulation differences are possible along broad-sloping carbonate shelves with mesophotic coral reef systems such as those in the USVI. This has direct implications for our general understanding of mesophotic coral reef carbonate basin development and the impact that sea level change can have. Specifically, carbonate deposits formed from reef growth at greater depths should not be modeled as having relatively homogeneous accretion.

The slow net average framework growth rates recorded in this study also provide some support to the traditional carbonate shelf theory that reef accretion decreases with depth (Schlager 1981, Bosscher & Schlager 1992). This support is increased when considering that the measured direct framework bioerosion rates were not quick enough to balance out deep- and shallow-water reefal carbonate accretion, as suggested by Hubbard (2009). However, results from this study do not account for benthic coverage and only considered the fate of coral carbonate covered by living polyp communities. Also, the actual geomorphological implications depend on the 3-dimensional spatial coverage of carbonate framework in the mesophotic coral reef habitats, as well as other carbonate-altering processes within the reef system. These various processes would best be addressed and compared in the form of a carbonate budget.

Acknowledgements. This research was funded by Sigma Xi, the National Science Foundation, the Geological Society of America, the Academy of Underwater Arts and Sciences, ExxonMobil, the University of Miami Center for Latin American Studies, the Leonard and Jayne Abess/Citizens Board, the RSMAS Graduate Student Fund, the Black Coral Penalty and Community Service Funds, the Virgin Islands Experimental Program to Stimulate Competitive Research (NSF #0814417), and the USVI TCRMP (#NA11NOS4820001). This is contribution 146 from the Center for Marine and Environmental Studies, University of the Virgin Islands. Special appreciation is given to P. Swart and the University of Miami Stable Isotope Laboratory, D. Marshall, A. Kuba, A. Frazier, C. Gil, and L. Chorniak for analytical support, and A. Weinstein for editorial review. Technical diving and boat support was provided by R. Gomez, E. Kadison, M. Kammann, and others from the University of the Virgin Islands. Helpful and constructive comments from the anonymous reviewers were greatly appreciated and highly contributed to improving the final version.

LITERATURE CITED

Aller RC, Dodge RE (1974) Animal–sediment relations in a tropical lagoon: Discovery Bay, Jamaica. J Mar Res 32: 209–232

Armstrong RA, Singh H, Torres J, Nemeth RS and others (2006) Characterizing the deep insular shelf coral reef habitat of the Hind Bank Marine Conservation District (US Virgin Islands) using the seabed autonomous underwater vehicle. Cont Shelf Res 26:194–205

Atkinson MJ, Carlson B, Crow GL (1995) Coral growth in high-nutrient, low-pH seawater: a case study of corals cultured at the Waikiki Aquarium, Honolulu, Hawaii. Coral Reefs 14:215–223

Bak RPM, Nieuwland G, Meesters E (2005) Coral reef crisis in deep and shallow reefs: 30 years of constancy and change in reefs of Curacao and Bonaire. Coral Reefs 24: 475–479

Bak RPM, Nieuwland G, Meesters EH (2009) Coral growth rates revisited after 31 years: What is causing lower extension rates in *Acropora palmata*? Bull Mar Sci 84: 287–294

Baker PA, Weber JN (1975) Coral growth rate: variation with depth. Earth Planet Sci Lett 27:57–61

Barnes DJ, Devereux MJ (1988) Variations in skeletal architecture associated with density banding in the hard coral *Porites*. J Exp Mar Biol Ecol 121:37–54

Bates NR, Best MHP, Neely K, Garley R, Dickson AG, Johnson RJ (2012) Detecting anthropogenic carbon dioxide uptake and ocean acidification in the North Atlantic Ocean. Biogeosciences 9:2509–2522

Bongaerts P, Ridgway T, Sampayo EM, Hoegh-Guldberg O (2010) Assessing the 'deep reef refugia' hypothesis: focus on Caribbean reefs. Coral Reefs 29:309–327

Bongaerts P, Muir P, Englebert N, Bridge TCL, Hoegh-Guldberg O (2013) Cyclone damage at mesophotic depths on Myrmidon Reef (GBR). Coral Reefs 32:935

Bosscher H, Meesters EH (1993) Depth related changes in the growth rate of *Montastrea annularis*. Proc 7th Int Coral Reef Symp 1:507–512

Bosscher H, Schlager W (1992) Computer simulation of reef growth. Sedimentology 39:503–512

Brandtneris VW, Brandt ME, Glynn PW, Gyory J, Smith TB (2016) Seasonal variability in calorimetric energy content of two Caribbean mesophotic corals. PLOS ONE 11: e0151953

Bridge T, Beaman R, Done T, Webster J (2012) Predicting the location and spatial extent of submerged coral reef habitat in the Great Barrier Reef World Heritage Area, Australia. PLOS ONE 7:e48203

Bruggemann JH, van Kessel AM, van Rooij JM, Breeman AM (1996) Bioerosion and sediment ingestion by the Caribbean parrotfish *Scarus vetula* and *Sparisoma viride*: implications of fish size, feeding mode and habitat use. Mar Ecol Prog Ser 134:59–71

Bucher DJ, Harriott VJ, Roberts LG (1998) Skeletal micro-density, porosity and bulk density of acroporid corals. J Exp Mar Biol Ecol 228:117–136

Carricart-Ganivet JP, Merino M (2001) Growth responses of the reef-building coral *Montastraea annularis* along a gradient of continental influence in the southern Gulf of Mexico. Bull Mar Sci 68:133–146

Carriquiry JD, Risk MJ, Schwarcz HP (1994) Stable isotope geochemistry of corals from Costa Rica as proxy indicator of the El Niño/Southern Oscillation (ENSO). Geochim Cosmochim Acta 58:335–351

Chalker BE, Barnes DJ (1990) Gamma densitometry for the measurement of skeletal density. Coral Reefs 9:11–23

Chollett I, Mumby PJ (2012) Predicting the distribution of *Montastraea* reefs using wave exposure. Coral Reefs 31: 493–503

Chollett I, Müller-Karger FE, Heron SF, Skirving W, Mumby PJ (2012) Seasonal and spatial heterogeneity of recent sea surface temperature trends in the Caribbean Sea and southeast Gulf of Mexico. Mar Pollut Bull 64:956–965

Cooper GRJ, Cowan DR (2008) Comparing time series using wavelet-based semblance analysis. Comput Geosci 34: 95–102

Dávalos-Dehullu E, Hernández-Arana H, Carricart-Ganivet JP (2008) On the causes of density banding in skeletons of corals of the genus *Montastraea*. J Exp Mar Biol Ecol 365:142–147

De'ath G, Lough JM, Fabricius KE (2009) Declining coral calcification on the Great Barrier Reef. Science 323: 116–119

Dodge RE, Szmant AM, Garcia R, Swart PK, Forester A, Leder JJ (1993) Skeletal structural basis of density banding in the reef coral *Montastrea annularis*. Proc 7th Int Coral Reef Symp 1:186–195

Dustan P (1975) Growth and form in the reef building coral *Montastrea annularis*. Mar Biol 33:101–107

Dustan P, Doherty O, Pardede S (2013) Digital reef rugosity estimates coral reef habitat complexity. PLOS ONE 8: e57386

Fairbanks RG, Dodge RE (1979) Annual periodicity of the $^{18}O/^{16}O$ and $^{13}C/^{12}C$ ratios in the coral *Montastrea annularis*. Geochim Cosmochim Acta 43:1009–1020

Felis T, Pätzold J, Loya Y, Wefer G (1998) Vertical water mass mixing and plankton blooms recorded in skeletal stable carbon isotopes of a Red Sea coral. J Geophys Res, C, Oceans 103:30731–30739

Ferrier-Pagès C, Gattuso JP, Dallot S, Jaubert J (2000) Effect of nutrient enrichment on growth and photosynthesis of the zooxanthellate coral *Stylophora pistillata*. Coral Reefs 19:103–113

Giannini A, Kushnir Y, Cane MC (2000) Interannual variability of Caribbean rainfall, ENSO, and the Atlantic Ocean. J Clim 13:297–310

Giannini A, Cane MA, Kushnir Y (2001) Interdecadal changes in the ENSO teleconnection to the Caribbean region and the North Atlantic Oscillation. J Clim 14: 2867–2879

Gladfelter EH, Monahan RK, Gladfelter WB (1978) Growth rates of five reef-building corals in the northeastern Caribbean. Bull Mar Sci 28:728–734

Gledhill DK, Wanninkhof R, Millero FJ, Eakin M (2008) Ocean acidification of the greater Caribbean region 1996–2006. J Geophys Res C Oceans 113:C10031

Glynn PW (1996) Coral reef bleaching: facts, hypotheses and implications. Glob Change Biol 2:495–509

Goldberg WM (1983) Cay Sal Bank, Bahamas: a biologically impoverished, physically controlled environment. Atoll Res Bull 271:1–17

Goreau TF (1959) The ecology of Jamaican coral reefs I. Species composition and zonation. Ecology 40:67–90

Goreau TF, Land LS (1974) Fore-reef morphology and depositional processes, north Jamaica. In: Laporte LF (ed) Reefs in time and space. Society of Economic Paleontologists and Mineralogists, Tulsa, OK, p 77–89

Graham NAJ, Wilson SK, Jennings S, Polunin NVC, Bijoux JP, Robinson J (2006) Dynamic fragility of oceanic coral reef ecosystems. Proc Natl Acad Sci USA 103:8425–8429

Grottoli AG (1999) Variability of stable isotopes and maximum linear extension in reef-coral skeletons at Kaneohe Bay, Hawaii. Mar Biol 135:437–449

Grottoli AG, Wellington GM (1999) Effect of light and zooplankton on skeletal $\delta^{13}C$ values in the eastern Pacific corals *Pavona clavus* and *Pavona gigantea*. Coral Reefs 18:29–41

Guzman HM, Cipriani R, Jackson JBC (2008) Historical decline in coral reef growth after the Panama Canal. Ambio 37:342–346

Harris PT, Bridge TCL, Beaman RJ, Webster JM, Nichol SL, Brooke BP (2013) Submerged banks in the Great Barrier Reef, Australia, greatly increase available coral reef habitat. ICES J Mar Sci 70:284–293

Helmle KP, Kohler KE, Dodge RE (2002) Relative optical densitometry and the coral X-radiograph densitometry

system: CoralXDS. Presented Poster. Int Soc Reef Studies 2002 European Meeting, Cambridge, England, Sept. 4–7
Helmle KP, Dodge RE, Swart PK, Gledhill DW, Eakin CM (2011) Growth rates of Florida corals from 1937 to 1996 and their response to climate change. Nat Commun 2: 215
Hoegh-Guldberg O, Mumby PJ, Hooten AJ, Steneck RS and others (2007) Coral reefs under rapid climate change and ocean acidification. Science 318:1737–1742
Holstein DM, Paris CB, Vaz AC, Smith TB (2015) Modeling vertical coral connectivity and mesophotic refugia. Coral Reefs 35:22–37
Houlbrèque F, Ferrier-Pagès C (2009) Heterotrophy in tropical scleractinian corals. Biol Rev Camb Philos Soc 84: 1–17
Hubbard DK (2009) Depth-related and species-related patterns of Holocene reef accretion in the Caribbean and western Atlantic: a critical assessment of existing models. In: Swart PK, Eberli GP, McKenzie JA, Jarvis I, Stevens T (eds) Perspectives in carbonate geology: a tribute to the career of Robert Nathan Ginsburg. John Wiley & Sons, Chichester, p 1–18
Hubbard DK, Scaturo D (1985) Growth rates of seven species of scleractinian corals from Cane Bay and Salt River, St. Croix, USVI. Bull Mar Sci 36:325–338
Hudson JH, Shinn EA, Halley RB, Lidz B (1976) Sclerochronology: a tool for interpreting past environments. Geology 4:361–364
Hughes TP (1987) Skeletal density and growth form of corals. Mar Ecol Prog Ser 35:259–266
Huston M (1985) Variation in coral growth rates with depth at Discovery Bay, Jamaica. Coral Reefs 4:19–25
James NP, Ginsburg RN (1979) The seaward margin of Belize barrier and atoll reefs: morphology, sedimentology, organism distribution and Late Quaternary history. International Association of Sedimentologists Special Publication No. 3. Blackwell Scientific Publications, Oxford
Jiang LQ, Feely RA, Carter BR, Greeley DJ, Gledhill DK, Arzayus KM (2015) Climatological distribution of aragonite saturation state in the global oceans. Global Biogeochem Cycles 29:1656–1673
Jones A, Berkelmans R (2010) Potential costs of acclimatization to a warmer climate: growth of a reef coral with heat tolerant vs. sensitive symbiont types. PLOS ONE 5: e10437
Kemp DW, Thornhill DJ, Rotjan RD, Iglesias-Prieto R, Fitt WK, Schmidt GW (2015) Spatially distinct and regionally endemic *Symbiodinium* assemblages in the threatened Caribbean reef-building coral *Orbicella faveolata.* Coral Reefs 34:535–547
Klotzbach PJ (2011) The influence of El Niño–Southern Oscillation and the Atlantic Multidecadal Oscillation on Caribbean tropical cyclone activity. J Clim 24:721–731
Kohler KE, Gill SM (2006) Coral point count with excel extensions (CPCe): a visual basic program for the determination of coral and substrate coverage using random point count methodology. Comput Geosci 32:1259–1269
Kwiatkowski L, Cox PM, Economou T, Halloran PR and others (2013) Caribbean coral growth influenced by anthropogenic aerosol emissions. Nat Geosci 6:362–366
Le Campion-Alsumard T, Golubic S, Hutchings P (1995) Microbial endoliths in skeletons of live and dead corals: *Porites lobata* (Moorea, French Polynesia). Mar Ecol Prog Ser 117:149–157
Leichter JJ, Genovese SJ (2006) Intermittent upwelling and subsidized growth of the scleractinian coral *Madracis mirabilis* on the deep fore-reef slope of Discovery Bay, Jamaica. Mar Ecol Prog Ser 316:95–103
Lenihan HS, Adjeroud M, Kotchen MJ, Hench JL, Nakamura T (2008) Reef structure regulates small-scale spatial variation in coral bleaching. Mar Ecol Prog Ser 370: 127–141
Lesser MP, Slattery M, Stat M, Ojimi M, Gates RD, Grottoli A (2010) Photoacclimatization by the coral *Montastraea cavernosa* in the mesophotic zone: light, food, and genetics. Ecology 91:990–1003
Little AF, van Oppen MJH, Willis BL (2004) Flexibility in algal endosymbioses shapes growth in reef corals. Science 304:1492–1494
Locker S, Armstrong R, Battista T, Rooney J, Sherman C, Zawada D (2010) Geomorphology of mesophotic coral ecosystems: current perspectives on morphology, distribution, and mapping strategies. Coral Reefs 29:329–345
Macdonald IA, Perry CT (2003) Biological degradation of coral framework in a turbid lagoon environment, Discovery Bay, north Jamaica. Coral Reefs 22:523–535
McClain CR, Barry JP (2010) Habitat heterogeneity, disturbance, and productivity work in concert to regulate biodiversity in deep submarine canyons. Ecology 91: 964–976
Millero FJ, Huang F (2009) The density of seawater as a function of salinity (5 to 70 g kg^{-1}) and temperature (273.15 to 363.15 K). Ocean Sci 5:91–100
Moses CS, Helmle KP, Swart PK, Dodge RE, Merino SE (2003) Pavements of *Siderastrea radians* on Cape Verde reefs. Coral Reefs 22:506
Perry CT, Spencer T, Kench PS (2008) Carbonate budgets and reef production states: a geomorphic perspective on the ecological phase-shift concept. Coral Reefs 27: 853–866
Pettay DT, Wham DC, Smith RT, Iglesias-Prieto R, LaJeunesse TC (2015) Microbial invasion of the Caribbean by an Indo-Pacific coral zooxanthella. Proc Natl Acad Sci USA 112:7513–7518
Pratchett MS, Anderson KD, Hoogenboom MO, Widman E and others (2015) Spatial, temporal and taxonomic variation in coral growth — implications for the structure and function of coral reef ecosystems. In: Hughes RN, Hughes DJ, Smith IP, Dale AC (eds) Oceanograpny and marine biology: an annual review. CRC Press, Boca Raton, FL, p 215–295
R Core Team (2014) R: a language and environment for statistical computing. R Foundation for Statistical Computing, Vienna, www.R-project.org
Randall JE (1974) The effect of fishes on coral reefs. Proc 2nd Coral Reef Symp 2(1):159–166
Riegl B, Piller WE (2003) Possible refugia for reefs in times of environmental stress. Int J Earth Sci 92:520–531
Rivera J, Prada M, Arsenault JL, Moody G, Benoit N (2006) Detecting fish aggregations from reef habitats mapped with high resolution side scan sonar imagery. NOAA Professional Paper NMFS 5:88–104
Roberts CM, Ormond RFG (1987) Habitat complexity and coral reef fish diversity and abundance on Red Sea fringing reefs. Mar Ecol Prog Ser 41:1–8
Ropelewski CF, Jones PD (1987) An extension of the Tahiti–Darwin Southern Oscillation Index. Mon Weather Rev 115:2161–2165
Rowan R, Knowlton N (1995) Intraspecific diversity and eco-

logical zonation in coral–algal symbiosis. Proc Natl Acad Sci USA 92:2850–2853

Runnalls LA, Coleman ML (2003) Record of natural and anthropogenic changes in reef environments (Barbados West Indies) using laser ablation ICP-MS and sclerochronology on coral cores. Coral Reefs 22:416–426

Saenger C, Cohen AL, Oppo DW, Halley RB, Carilli JE (2009) Surface-temperature trends and variability in the low-latitude North Atlantic since 1552. Nat Geosci 2: 492–495

Schlager W (1981) The paradox of drowned reefs and carbonate platforms. Geol Soc Am Bull 92:197–211

Schoepf V, Levas SJ, Rodrigues LJ, McBride MO and others (2014) Kinetic and metabolic isotope effects in coral skeletal carbon isotopes: a re-evaluation using experimental coral bleaching as a case study. Geochim Cosmochim Acta 146:164–178

Scoffin TP, Stearn CW, Boucher D, Frydl P, Hawkins CM, Hunter IG, MacGeachy JK (1980) Calcium carbonate budget of a fringing reef on the west coast of Barbados. Part II. Erosion, sediments and internal structure. Bull Mar Sci 3:475–508

Scoffin TP, Tudhope AW, Brown BE, Chansang H, Cheeney RF (1992) Patterns and possible environmental controls of skeletogenesis of *Porites lutea*, south Thailand. Coral Reefs 11:1–11

Sharifi A, Pourmand A, Canuel EA, Ferer-Tyler E and others (2015) Abrupt climate variability since the last deglaciation based on a high-resolution, multi-proxy peat record from NW Iran: the hand that rocked the cradle of civilization? Quat Sci Rev 123:215–230

Sheppard C, Rioja-Nieto R (2005) Sea surface temperature 1871–2099 in 38 cells in the Caribbean region. Mar Environ Res 60:389–396

Shimamura M, Irino T, Oba T, Xu G, Lu B, Wang L, Toyoda K (2008) Main controlling factors of coral skeletal carbon isotopic composition and skeletal extension rate: high-resolution study at Hainan Island, South China Sea. Geochem Geophys Geosyst 9, Q04024

Slattery M, Lesser MP, Brazeau D, Stokes MD, Leichter JJ (2011) Connectivity and stability of mesophotic coral reefs. J Exp Mar Biol Ecol 408:32–41

Smith LW, Barshis D, Birkeland C (2007) Phenotypic plasticity for skeletal growth, density and calcification of *Porites lobata* in response to habitat type. Coral Reefs 26: 559–567

Smith TB, Nemeth RS, Blondeau J, Calnan JM, Kadison E, Herzlieb S (2008) Assessing coral reef health across onshore to offshore stress gradients in the US Virgin Islands. Mar Pollut Bull 56:1983–1991

Smith TB, Blondeau J, Nemeth RS, Pittman SJ, Calnan JM, Kadison E, Gass J (2010) Benthic structure and cryptic mortality in a Caribbean mesophotic coral reef bank system, the Hind Bank Marine Conservation District, U.S. Virgin Islands. Coral Reefs 29:289–308

Smith TB, Brandt ME, Calnan JM, Nemeth RS and others (2013) Convergent mortality responses of Caribbean coral species to seawater warming. Ecosphere 4:art87

Smith TB, Kadison E, Ennis RS, Gyory J and others (2014) The United States Virgin Islands Territorial Coral Reef Monitoring Program. Year 14 Annual Report. Version 1. University of the Virgin Islands, Charlotte Amalie, USVI

Smith TB, Brandtneris VW, Canals M, Brandt ME and others (2016a) Potential structuring forces on a shelf edge upper mesophotic coral ecosystem in the US Virgin Islands. Front Mar Sci 3:115

Smith TB, Gyory J, Brandt ME, Miller WJ, Jossart J, Nemeth RS (2016b) Caribbean mesophotic coral ecosystems are unlikely climate change refugia. Glob Change Biol 22: 2756–2765

Spencer Davies P (1989) Short-term growth measurements of corals using an accurate buoyant weighing technique. Mar Biol 101:389–395

Stambler N, Popper N, Dubinsky Z, Stimson J (1991) Effects of nutrient enrichment and water motion on the coral *Pocillopora damicornis*. Pac Sci 45:299–307

Stearn CW, Scoffin TP (1977) Carbonate budget of a fringing reef, Barbados. Proc 3rd Int Coral Reef Symp 2: 471–476

Swart PK (1983) Carbon and oxygen isotope fractionation in scleractinian corals: a review. Earth Sci Rev 19:51–80

Swart PK, Dodge RE, Hudson HJ (1996) A 240-year stable oxygen and carbon isotopic record in a coral from south Florida: implications for the prediction of precipitation in southern Florida. Palaios 11:362–375

Tanzil JTI, Brown BE, Dunne RP, Lee JN, Kaandorp JA, Todd PA (2013) Regional decline in growth rates of massive *Porites* corals in southeast Asia. Glob Change Biol 19:3011–3023

Tartaglione CA, Smith SR, O'Brien JJ (2003) ENSO impact on hurricane landfall probabilities for the Caribbean. J Clim 16:2925–2930

Tomascik T (1990) Growth rates of two morphotypes of *Montastrea annularis* along a eutrophication gradient, Barbados, W.I. Mar Pollut Bull 21:376–381

Torrence C, Compo GP (1998) A practical guide to wavelet analysis. Bull Am Meteorol Soc 79:61–78

Torres JL, Morelock J (2002) Effect of terrigenous sediment influx on coral cover and linear extension rates of three Caribbean massive coral species. Caribb J Sci 38: 222–229

Torres E, Colominas MA, Schlotthauer G, Flandrin P (2011) A complete ensemble empirical mode decomposition with adaptive noise. IEEE Int Conf on Acoustics, Speech and Signal Processing (ICASSP) 4144–4147

Van Veghel MLJ, Bosscher H (1995) Variation in linear growth and skeletal density within the polymorphic reef building coral *Montastrea annularis*. Bull Mar Sci 56: 902–908

Vogel K, Gektidis M, Golubic S, Kiene WE, Radtke G (2000) Experimental studies on microbial bioerosion at Lee Stocking Island, Bahamas, and One Tree Island, Great Barrier Reef, Australia: implications for paleoecological reconstructions. Lethaia 33:190–204

Weber J (1974) $^{13}C/^{12}C$ ratios as natural isotopic tracers elucidating calcification processes in reef-building and non-reef-building corals. Proc 2nd Int Symp Coral Reefs 2: 289–298

Weinstein DK, Klaus JS, Smith TB (2014) Mesophotic bioerosion: variability and structural impact on U.S. Virgin Island deep reefs. Geomorphology 222:14–24

Weinstein DK, Klaus JS, Smith TB (2015) Habitat heterogeneity reflected in mesophotic reef sediments. Sediment Geol 329:177–187

White KN, Ohara T, Fujii T, Kawamura I and others (2013) Typhoon damage on a shallow mesophotic reef in Oki-

Editorial responsibility: James McClintock, Birmingham, Alabama, USA

Submitted: February 5, 2016; Accepted: August 26, 2016
Proofs received from author(s): October 26, 2016